



# Technical Report

Team #13

Aachen Drone Development Initiative



## ADDI

Aachen Drone Development Initiative

# Contents

<b>1</b>	<b>Introduction</b>	<b>2</b>
<b>2</b>	<b>Rules</b>	<b>3</b>
<b>3</b>	<b>Project Management</b>	<b>4</b>
3.1	Team Structure . . . . .	4
3.2	Milestones . . . . .	5
3.3	Meeting Structure . . . . .	5
3.4	Finances . . . . .	5
<b>4</b>	<b>Aerodynamic Design and Aircraft Optimization</b>	<b>7</b>
4.1	First optimization step . . . . .	8
4.2	Second optimization step . . . . .	11
4.3	Calculation and Design Methods . . . . .	13
4.3.1	Empennage geometry . . . . .	13
4.3.2	Fuselage geometry . . . . .	13
4.3.3	Mass calculation . . . . .	14
4.3.4	Take-off calculation . . . . .	15
<b>5</b>	<b>Structural Design and Manufacturing</b>	<b>16</b>
5.1	Description of Used Manufacturing Techniques . . . . .	16
5.2	Wing . . . . .	17
5.3	Empennage . . . . .	19
5.4	Landing Gear . . . . .	19
5.5	Fuselage . . . . .	20
5.6	Payload Prediction . . . . .	21
<b>6</b>	<b>Electronic Components</b>	<b>22</b>
6.1	Battery . . . . .	22
6.2	Servomotors . . . . .	22
<b>7</b>	<b>Testing</b>	<b>24</b>
7.1	Propeller Selection . . . . .	25
7.2	Validation of QPROP calculations . . . . .	25
7.3	Determination of voltage levels depending on battery capacity . . . . .	26
<b>8</b>	<b>Outlook</b>	<b>28</b>
	<b>Bibliography</b>	<b>29</b>

# 1 Introduction

The Aachen Drone Development Initiative e.V. (ADDI) is an association of 30 students at the RWTH Aachen University. We work on a wide range of projects from autonomous drones, solar airplanes and conventional aircraft optimization like the Air Cargo Challenge 2022. The seven members of our team have a broad spectrum of fields of study, from business to energy and aerospace engineering. What brings us together is the passion for aviation and unmanned aircraft. While some of us are long lasting members since the founding days of ADDI in 2018, we also have some new team members, who joined in the recent months.

The Air Cargo Challenge, held in Munich this year, provides an excellent opportunity for every one of us to learn. Not only can we apply the rather theoretical knowledge from our studies to the real world, but we also learn how to deal with various difficulties. Apart from development itself, the ongoing covid crisis has been a major hardship, that not only we as a team, but our competitors as well are facing continuously. Furthermore, the pandemic left its marks on the aviation industry as a whole, which made getting required sponsoring and financial support, necessary for the success of our project, a big issue. Fortunately, we have been able to overcome these obstacles, leaving us more than excited to finally be able to fly and compete this summer.

## 2 Rules

In the following, the regulations of the Air Cargo Challenge are briefly summarized. The main aspect of the competition is the transport of blood bags by an unmanned aircraft. The flight task consists of four segments: take-off, climb, cruise flight and landing. Taking off on a grass runway, the maximum takeoff distance must not exceed 60 m. In the subsequent 60 s climb, the aircraft should ascend as close as possible to an altitude of 100 m. This is followed by a 120 s cruise flight, during which the maximum possible distance must be covered. The flight route can be freely selected within a certain flight corridor. The landing is not part of the evaluation.

The aircraft size is limited by two requirements. In all flight configurations, the aircraft has to fit into a rhombus shaped box with an edge length of 1500 mm and a height of 500 mm. The rhombus angle can be freely selected. Additionally, all aircraft components have to fit into a box with the dimensions of 1100 × 400 × 250 mm<sup>3</sup> for transportation. This can be achieved with an appropriately sized aircraft or through disassembly. Furthermore, the rules require a specific combination of motor, propeller and battery voltage.

The flight competition consists of several rounds of flying. Each team can fly once per round and the mission score of each round depends on several factors like payload amount, flown distance and altitude after the climb. The determination of the respective score is then obtained by normalization with the best achieved value of the round of all teams participating. In addition, the time for loading and unloading, the accuracy of a payload prediction and the length of the used runway are included in the mission score. By using equation 2.1, the total points per team per round are calculated. Following all rounds, the overall mission score is calculated by adding up the points of each, divided by the number of rounds in which the team flew.

$$S_{\text{Round},N} = B_{\text{takeoff}} \left( \frac{S_{\text{payload}} + S_{\text{dist}} + S_{\text{altitude}}}{3} + (B_{\text{Load}} + B_{\text{Unload}} + B_{\text{Prediction}}) \right) \quad (2.1)$$

The overall Air Cargo Challenge score consists not only of the mission score, but also of other deliverables. These include a video presentation, drawings and this technical report.

## 3 Project Management

In this chapter our team organization, financial budgeting and time schedule are outlined. The team consists of seven people from our student initiative. Our initiative has participated in other competitions before but the rules and goals regarding the aircraft design and manufacturing were new to all of us.

### 3.1 Team Structure

The team's general structure consists of a team leader, a technical leader and department leads. The team leader is responsible for organisation and general progress of the project. For all technical aspects, the technical lead is accountable and the department leads are responsible for their specific areas like manufacturing and propulsion. This structure (Figure 3.1) ensures clear information flow and defined responsibilities. In the process of building the aircraft every team member is involved and there are no purely management positions. Experience was advantageous but not needed for a member to be responsible for a task.

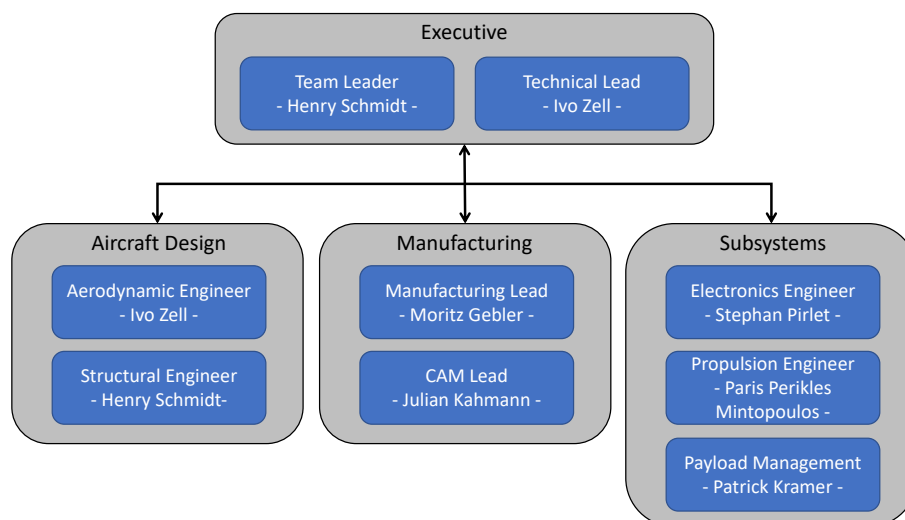


**Figure 3.1:** Team Structure

## 3.2 Milestones

At the beginning of the Air Cargo Challenge project, milestones were defined by the lead management based on the rules and experiences from previous competitions. Each team member decided which subject they wanted to work on. The milestones were adjusted during the project and the final milestones are shown in figure 3.2.

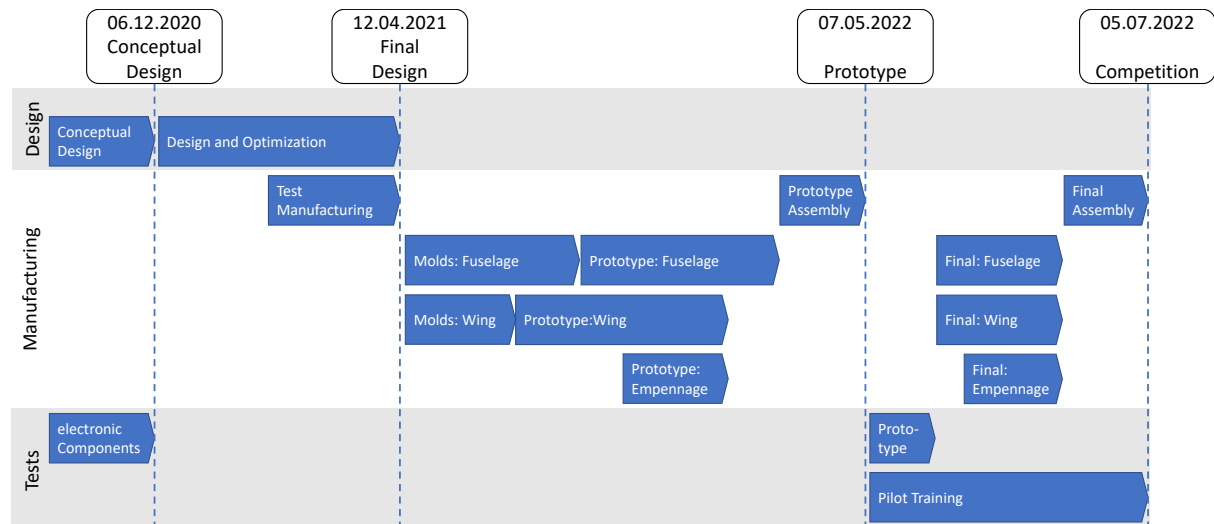


Figure 3.2: Timeline

## 3.3 Meeting Structure

In a weekly online meeting, we exchanged and archived information about the progress made by the individual departments and the overall project progress to update every team member. Therefore, the milestones were reviewed and the short-term goals for the following week were set. During the construction phase, which is still ongoing, we are working in our workshop twice a week on the competition model to build it and develop it further.

## 3.4 Finances

The financing of the Air Cargo Challenge participation is explained below. In total, the costs for the participation amount to 13700€. The breakdown is shown in table 3.1. Furthermore, we were able to convince various sponsors to support us. The amount of these sponsorships and the summary of the total funding are also shown in table 3.1.

Position	Description	
<b>Competition costs</b>	<b>3,520 €</b>	
Competition tickets	2,650 €	7 team member + 3 guests
Train tickets	750 €	10 tickets, each 75 €
Transfer	120 €	10 transfer, each 12 €
<b>Material</b>	<b>4,180 €</b>	
Fiber material	1,600 €	Carbon/glas fiber, epoxy resin, ...
Mold material	400 €	MDF plates
Other material	600 €	3D print material, CFK tubes, ...
Batteries	380 €	High performance LiPo batteries
Electronic components	950 €	Motor, ESC, servos
Tools	150 €	
Other	100 €	Cables, screws, connectors
<b>Running Costs</b>	<b>6,000 €</b>	
Workshop rent	5,400 €	12 month each 450 € (warm rent incl. internet)
Insurances	600 €	12 month each 50 €
<b>Total Costs</b>	<b>13,700 €</b>	
<b>Sponsors</b>		
Autodesk	8,000 €	Sponsoring
Hans Hermann Voss Stiftung	5,400 €	Support
3D-Filament	450 €	3D print filament
Carbonteam	150 €	CFK tubes
Interglas	500 €	Glas fiber material
Teijin	500 €	CFK rovings
Holybro	500 €	RC-Equipment
<b>Total Budget</b>	<b>15,500 €</b>	

**Table 3.1:** Cost Breakdown

In summary, we are sufficiently financed to travel to the Air Cargo Challenge with 7 team members and 3 guests. We are especially grateful to Autodesk and the Hans Hermann Voss Stiftung for supporting us generously. Nevertheless, it was extremely difficult to get material sponsors from the struggling aviation industry this year. In addition, a sponsorship of carbon fiber materials could not be realized due to a shortage of raw materials.

## 4 Aerodynamic Design and Aircraft Optimization

For the preliminary design, an optimization program was developed aiming at maximizing the score achieved in the competition. The core of this program is a meta-heuristic optimizing algorithm in combination with a calculation model for the achieved score.

Because the computation time of meta-heuristic algorithms increases exponentially with the number of parameters, the entire process was divided into two steps. The first step provides a first sizing of the aircraft and is comparable to the conceptual design. The second step is similar to the preliminary design and mainly optimizes the wing geometry.

The meta-heuristic optimization algorithm needs three input elements. First, the parameters to be optimized are defined. Second, upper and lower limits are specified for each parameter. Last, the objective function is defined. The objective function calculates the aircraft performance depending on the values of the parameters.

Before the optimization problem was set up, three design decisions were made:

1. a conventional aircraft configuration was chosen because it is the most proven configuration, allows a wide range of speed and is best represented by the used methods.
2. tricycle landing gear was chosen to minimize the angle of attack during take-off to minimize drag. In addition, the aircraft can rotate quickly at take-off.
3. dihedral of  $2^\circ$  based on experience on comparable model aircrafts in this size [8].

## 4.1 First optimization step

The first optimization step uses eight parameters, which are summarized in the vector

$$\vec{x}_I = (m_{\text{payload}}, \beta, c_{\text{root}}, x_{\text{trailingedge}}, C, d_{\text{wing}}, w_{\text{wing}}, d_{\text{empairfoil}}), \quad (4.1)$$

which are explained in detail in this section.

The payload mass  $m_{\text{payload}}$  directly influences the flight point score and the total mass. A rectangular wing is assumed in the first step and the rhombus angle  $\beta$  determines the aircraft length and wingspan. The chord length  $c_{\text{root}}$  has a direct influence on the Reynolds number and thus the viscous drag. Furthermore, the position of the trailing edge  $x_{\text{trailingedge}}$  of the wing is defined, which has an influence on the position of the center of gravity and the distance between wing and empennage. The battery capacity  $C$  is chosen as a propulsion parameter. With increasing capacity, the discharge rate decreases which increases the voltage level. However, a larger battery capacity increases the total mass. To define the airfoil characteristics in terms of viscous drag of the wing and empennage, averaged data is used depending on airfoil thickness  $d$  and airfoil camber  $w$ . The averaged data is read from a database with more than 2300 airfoils calculated with XFOIL [4] based on airfoil thickness and camber.

First, the complete aircraft geometry is derived from the values proposed by the optimization algorithm. The parameterization is shown in figure 4.1.

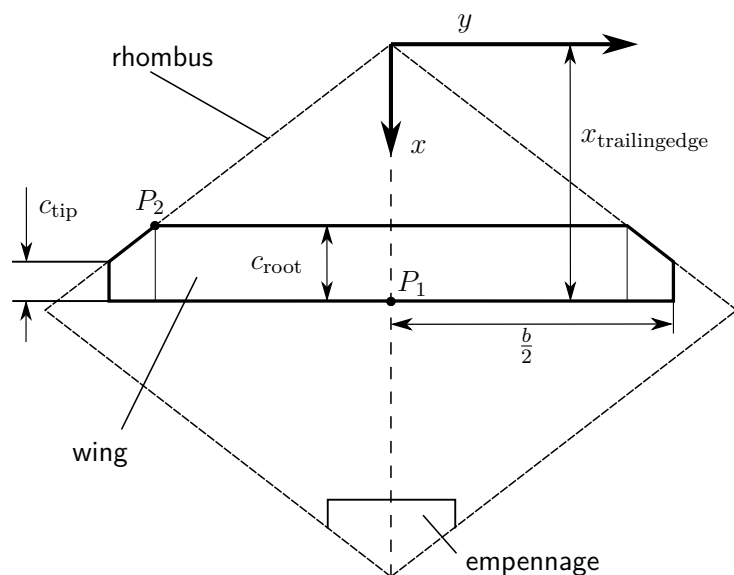


**Figure 4.1:** Parametrization of the wing geometry in the first step within the rhombus.

The empennage is placed in the very back corner of the rhombus. The center of gravity is set to 30% of the wing chord to determine the payload position and size of fuselage. The methods for empennage and fuselage sizing are the same in step 1 and 2. They are explained separately in section 4.3.1 and 4.3.2. Before the objective function calculates the flight performance or the number of flight points from the aircraft geometry, the values are controlled for adequacy with termination conditions. If the combination of the values lies within the permitted values, the mass calculation follows. The mass calculations, explained in more detail in section 4.3.3, are also equal within step 1 and 2.

Subsequently, the flight performance calculation is conducted. First, the take-off length is calculated, which is explained in section 4.3.4. If the take-off distance exceeds 60 m the calculation is aborted. For climb and cruise, a Lilienthal polar of the airplane is calculated. The drag coefficient  $C_{D, \text{total}}$  results from the sum of  $C_{D, \text{wing}}$ ,  $C_{D, \text{emp}}$ , and  $C_{D, \text{fuselage}}$ , which use wing area as reference. The viscous parts of  $C_{D, \text{wing}}$  and  $C_{D, \text{emp}}$  are read from the airfoil database based on airfoil thickness and camber. The fuselage drag is obtained from the cross-sectional area, which results from the payload volume, and a  $C_{d, \text{fuselage}} = 0.8$  [5], which is assumed as constant. The induced drag of the wing and empennage is determined by equation 4.2 [6] for the Oswald factor  $e$  as a function of the aspect ratio  $\Lambda$ .

$$e = 1.78(1 - 0.045\Lambda^{0.69}) - 0.64 \quad (4.2)$$

In addition, a parasitic drag correction factor of 1.1 for the total drag is assumed. After the Lilienthal polar has been determined, the propulsive power is calculated. For this purpose, the flight is divided into three segments: take-off, climb and cruise. In each segment, the battery voltage and therefore also the propulsion power decreases depending on the battery capacity  $C$ . Using the program QPROP [2], the propulsion power was calculated using a propeller and motor model.

Figure 4.2 shows the power polars of the aircraft which are calculated via the relation

$$P_{\text{needed}} = Wv = \frac{\rho}{2} S_{\text{ref}} C_D v^3. \quad (4.3)$$

The highest rate of climb results from the maximum power difference between propulsion power and required power for level flight. Thus, at this point of maximum power difference, the speed for climb can be determined. The cruise speed is a result of the intersection of the propulsion power and the required power. The climb speed is given by

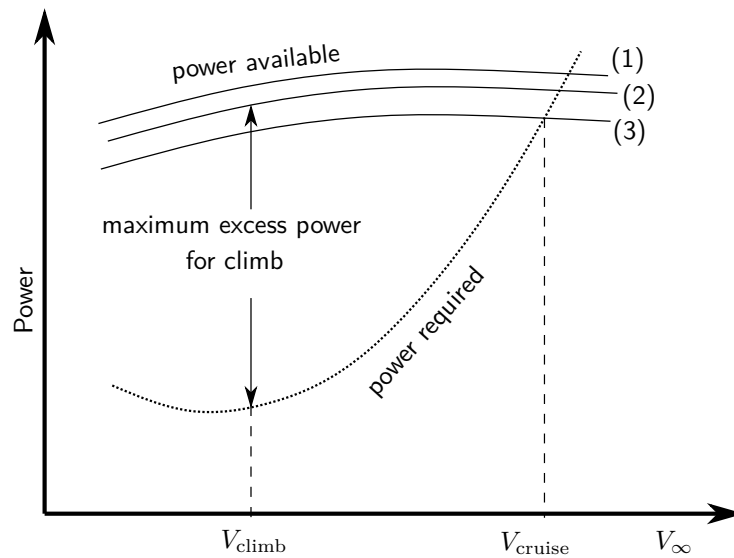


**Figure 4.2:** Determination of speed in climb and cruise. The available power during take-off (1), climb (2) and cruise (3) is plotted schematically over speed.

$$v_{z,\text{climb}} = \frac{\text{excess power}}{\text{total mass} \cdot g} \quad (4.4)$$

proposed by ANDERSON [1]. Thus, the two operating points of climb and cruise are read from figure 4.2. Finally, the achievable score is determined by the score equation 2.1 and returned to the meta-heuristic algorithm. The algorithm evaluates the result and converges to a proposed solution within a given number of iterations. The best result generated by the algorithm for the used approach in the first optimization step is shown in table 4.1.

$m_{\text{payload}}$	3.047 kg
$\beta$	80.75°
$c_{\text{root}}$	0.243 m
$x_{\text{trailingedge}}$	1.183 m
$C$	3.56 A h
$d_{\text{wingairfoil}}$	5 %
$w_{\text{wingairfoil}}$	2 %
$d_{\text{empairfoil}}$	5 %
chosen wing airfoil	ag19
chosen empennage airfoil	goe443
chosen battery	4 A h

**Table 4.1:** The best result of the first optimization step.

Based on the results of the first optimization step, an airfoil selection is made for the wing and empennage. The wing-airfoil has a thickness of 5% and a camber of 2% according to the optimization results. The airfoil of the empennage is symmetrical and also has a thickness of

5%. For comparison,  $C_{d,climb}$  and  $C_{d,cruise}$  are determined in an environment of  $C_l \pm 0.03$  at the Reynolds number known from the result from optimization step one. This ensures that the drag coefficient is also low around the operating point. Mark Drela's ag19 airfoil was chosen for the wing and the goe443 airfoil for the empennage. In addition, a selection is made from commercially available LiPo batteries based on the specified battery capacity in table 4.1.

## 4.2 Second optimization step

In the first step, a simple aircraft design with a rectangular wing planform was generated and supplemented by an airfoil selection. In the following second step, the limits of the parameter space are more restricted. Based on calculations using the vortex grid method, a more detailed design can be conducted and an optimized wing geometry can be returned. The optimization vector  $\vec{x}_{II}$  is determined thus the entire aircraft can be derived from as few design parameters as possible. This is followed by the calculation of the flight performance. For this purpose, the external programs XFOIL, QPROP and AVL are used automatically in combination with our additionally developed methods, which are explained in section 4.3.

The parameters in the second step are focused on the wing shape. The wing is defined by the angle of incidence, the geometric twist and seven further parameters determining the geometry of leading and trailing edge using Bézier curves. This parameterization is shown in figure 4.3.

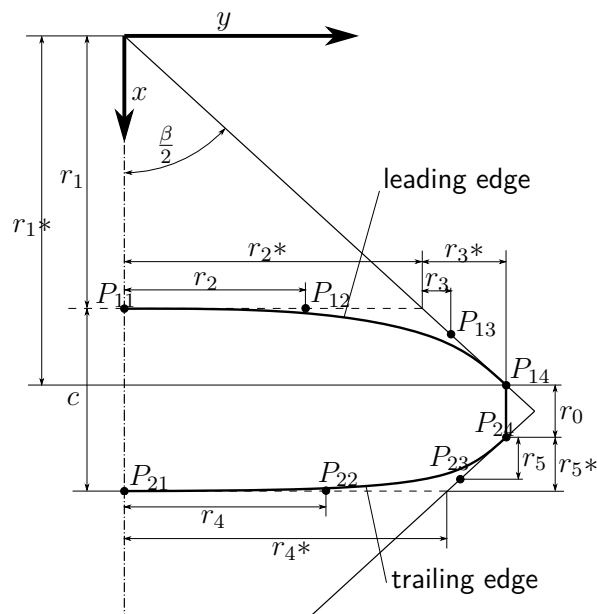


**Figure 4.3:** Relative parameterization of the wing in the second step based on Bézier curves.

In addition to the geometric wing parameters, the payload mass, the rhombus angle and the root chord are selected with upper and lower border set to  $\pm 20\%$  of the results of the first optimization step. The aerodynamic center of the configuration is determined with AVL [3]. In the second step, a stability margin of 15% is assumed. The position of the center of gravity can be determined with the established stability measure and the mean aerodynamic chord. Following this, the mass calculation is conducted which is explained separately in section 4.3.3.

After the complete airplane geometry and airplane mass have been determined on the basis of the parameter values, the airplane polar calculation is continued as in the first step. First, the lift distribution and  $C_{d,induced}$  are determined with AVL. The viscous drag coefficient at a wing segment results from the local lift coefficient and the local Reynolds number.  $C_{d,viscous}$  is interpolated between the segments. The rest of the flight performance and score calculation is the same procedure as in the first optimization step and will not be explained further.

The best plane geometry calculated in step two is shown in figure 4.4. The associated technical data is shown in table 4.2.

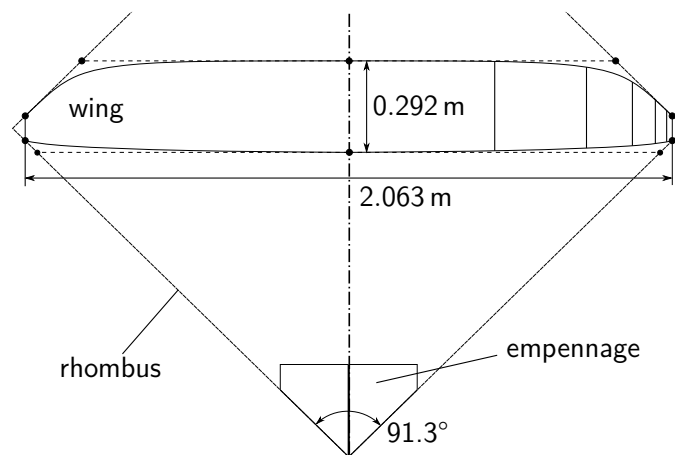


**Figure 4.4:** Wing and empennage geometry of the best position of the second step within the rhombus with an opening angle of  $\beta = 91.3^\circ$ .

The rhombus angle of  $91.3^\circ$  is very close to the maximum area of the rhombus. With a power surplus in climb of 123 W, a theoretical altitude of 102 m is reached. With a pilot factor of 0.8, the altitude is reduced to 82 m. In cruise flight with a speed of  $27.4 \frac{m}{s}$  a distance of 3 283 m is covered. The take-off distance is lower than 40 m to achieve the bonus multiplier.

The result of the second step forms the preliminary design of the competition model and thus the basis for the detail design, which is described in chapter 5.

$\beta$	91.3°
$m_{\text{total}}$	5.52 kg
$m_{\text{payload}}$	3.346 kg
$b$	2.06 m
$S_{\text{ref}}$	0.534 m <sup>2</sup>
wing loading	103.39 g/dm <sup>2</sup>
$v_{z,\text{climb}}$	1.82 m/s
$v_{\text{cruise}}$	27.4 m/s
$P_{\text{excess power}}$	123 W
$d_{\text{take-off}}$	39.9 m

**Table 4.2:** Results and technical data of the preliminary design

### 4.3 Calculation and Design Methods

The first and second optimization step explained in the last two sections partially share the same calculation and design methods which are described in the following. The empennage and fuselage sizing are presented qualitatively. In addition, the mass calculation and the take-off distance calculation are explained.

#### 4.3.1 Empennage geometry

The leading edge of the horizontal stabilizer is assumed to be straight. The projected horizontal tailplane area is given by RAYMER [6, p. 112] as

$$S_{\text{emp}} = \frac{c_H c_{\text{MAC,wing}} S_{\text{wing}}}{L_{\text{wing,emp}}} \quad (4.5)$$

where  $c_{\text{MAC,wing}}$  describes the mean aerodynamic chord,  $S_{\text{wing}}$  the wing area and  $L_{\text{wing,emp}}$  the distance between wing and empennage. The horizontal tailplane volume coefficient  $c_H$ , is given by RAYMER [6, p. 112] as 0.5 for man-carrying gliders. In THIES [8, p. 72],  $c_H = 0.6$  is suggested for RC glider models. A compromise  $c_H = 0.55$  is used as the mean value.

#### 4.3.2 Fuselage geometry

The fuselage parameters are derived from the optimization vector and the aircraft geometry. For this purpose, the center of gravity of the airplane is determined first. The center of gravity of the loaded payload should be located at the aircraft center of gravity  $x_{CG}$ .

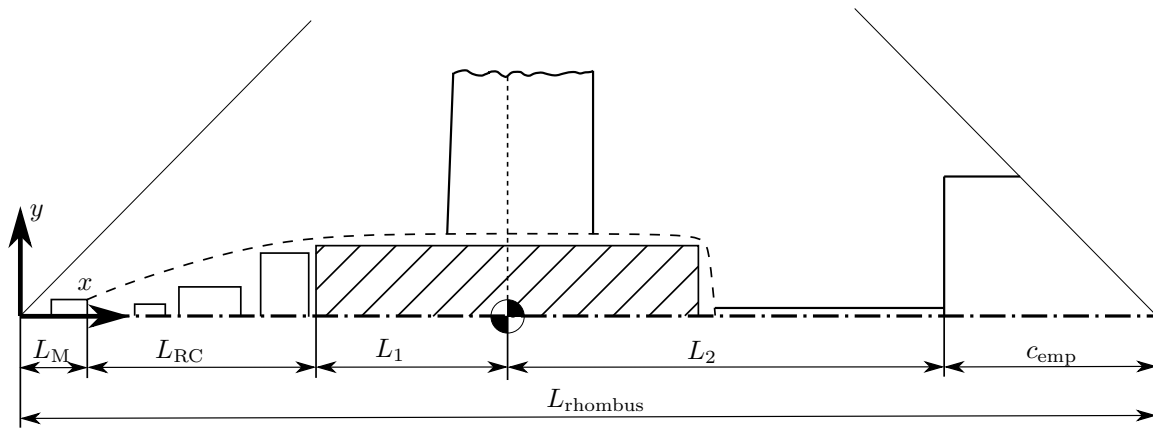


**Figure 4.5:** The airplane with plotted lengths of the different elements in  $x$ -direction to determine the payload length.

The length of the payload is shown in figure 4.5 and calculated with equation 4.6.

$$L_{\text{payload}} = 2 \cdot \min(x_{\text{CG}} - L_M - L_{\text{RC}}, L_{\text{Rhombus}} - x_{\text{CG}} - c_{\text{emp}}) \quad (4.6)$$

The fuselage is assumed as a cylinder which is determined by the fuselage diameter and cross section based on the the payload mass and the proportional payload volume.

### 4.3.3 Mass calculation

The total mass is calculated with equation 4.7.

$$m_{\text{total}} = a((m_{\text{other}} + m_{\text{wing}} + m_{\text{emp}})b + c) \quad (4.7)$$

Based on experience of previous projects, the correction factor  $a$  is set to 1.1 for additional glue, cables and other small parts. The parameters  $b = 1.00533$  and  $c = 0.01 \text{ kg}$  take the mass of the landing gear into account, which is chosen from COTS products.

The other masses are summed up to  $m_{\text{other}}$  which includes all electric components, the battery mass and the mass of the fuselage.

For the mass calculation of the wing, the lift distribution and the mass distribution are conservatively assumed as constant. Therefore, the resulting lift force acts at the quarter-span of the wing. The resulting lift force at one wing side is calculated by

$$L_{\text{res}} = g \cdot n_{\text{max}} \cdot \frac{m_{\text{other}}}{2}. \quad (4.8)$$

To simplify the mass calculation, the spar cap mass is determined from a simplified moment calculation and is skipped here because the exact design and calculation of the spar caps is carried out in chapter 5.2. The skin of the wing is determined by the composite layup, which is also described in 5.2. The spar and skin mass together result in the total wing mass  $m_{\text{wing}}$ . The mass calculation of the empennage is carried out analogous.

### 4.3.4 Take-off calculation

A special aspect of the regulations is, that a take-off distance of less than 40 m results in a bonus score multiplier of 1.1. Furthermore, the maximum allowed take-off distance is limited to 60 m.

The first step is to calculate the take-off velocity  $v_{\text{takeoff}}$  with  $v_{\text{stall}}$  [9, p.265][6, p.487].

$$v_{\text{take-off}} = 1.1 * v_{\text{stall}} = 1.1 * 0.94 * \sqrt{\frac{2 * m_{\text{total}}}{\rho * S_{\text{ref}} * 0.85 * C_{A,\text{max}}}} \quad (4.9)$$

The acceleration to this velocity is divided into multiple segments with a step size of 1 m/s. For each segment, the acceleration is calculated again based on thrust, aerodynamic drag and roll resistance with equation 4.10. The available thrust is computed by QPROP taking the air inflow velocity and battery voltage into account. The total take-off distance results from the sum of the segments.

$$a_i = \frac{S_{i+1} - D_{i+1} - \mu_R(m_{\text{total}}g - A_i)}{m_{\text{total}}} \quad (4.10)$$

## 5 Structural Design and Manufacturing

The main goal of the structural design of the aircraft is a lightweight airframe. For this purpose, all structural components are made from carbon and glass fiber composite which provides an excellent mass-to-strength ratio and allows the realisation of complex geometries. After the manufacturing process is introduced, the structural design of the components wing, empennage, landing gear and fuselage are presented.

### 5.1 Description of Used Manufacturing Techniques

The selection of materials and manufacturing processes is based on four criteria: costs, mechanical properties, the difficulty of manufacturing and the possibility to carry out fast iterative improvements. In the following, the used materials and manufacturing processes will be presented.

#### **Foam Core Composites**

The vacuum bagged foam core method is perfectly suited for quick and relatively easy manufacturing of aerodynamic shapes. It uses a hot-wire cut foam core which provides the basic shape of the wing. Structural reinforcements can be locally added if necessary, before the foam core is covered with carbon or glass fiber fabric. To firmly join the foam core and the skin, a vacuum bag is used to ensure good contact of the fabric to the core and a heated chamber can be used to improve the mechanical properties while hardening. A Mylar sheet between laminate and vacuum bag ensures a smooth surface of the outer skin. The advantages of this method are a very fast built time, which enables quick prototyping and testing of different airfoils, while providing fair structural properties with a adequate strength to weight ratio. Compared to the molded sandwich construction method the accuracy of the resulting shape is worse and the parts are heavier.

## Molded Sandwich Shell

For the manufacturing of a sandwich shell, a mold is created for the external shape of the component. Molds can be made in several ways. A cheap solution are molds milled from MDF board. MDF is a readily available and cheap material. Multiple MDF boards are glued together to create a mold blank. These blanks are machined using a CNC router. In the first machining step the blank is roughed down to its final shape with 0.2 mm being left on all important mold surfaces. Then the mold is covered in epoxy resin which is absorbed into the surface of the MDF. After hardening, the resin infused MDF is machined again, now to its final dimensions. After the second machining multiple steps of sanding, polishing and waxing are needed to acquire the necessary surface finish. A mold might need to be machined in multiple parts which are glued together after the final machining to account for limited manufacturing capabilities.

Another option is the utilization of fused filament fabrication 3D printing. This method is very easy and cheap to realise but requires a lot of work to achieve a good surface finish. The resulting mold is also substantially less accurate than the previous mentioned method. Due to the limited size of 3D printers the mold might need to be split into multiple parts which are glued together after printing. First, a two component polyester filler is used to even out the transition of the individually printed parts. Then a spray on polymer filler is used to even out the surface. Both fillers are applied multiple times with intermediate sanding. Then the molds are polished and waxed. These molds cannot be used with vacuum bags due to their low strength and have to be protected from heat since it can cause warping.

To manufacture the aircraft components, several layers of glass or carbon fiber fabrics as well as sandwich materials, like lightweight Airex foam, are placed in the molds and impregnated with epoxy resin. The resin then cures over time during which heat can be applied to improve mechanical properties and a vacuum can be used to ensure perfect compression of the materials and adhesion to the mold. When using a vacuum, a felt fabric can be used to soak up excess resin and thus decrease the weight. This process results in optimum strength-to-weight ratios and high surface quality. However, the effort required to create the molds is much higher compared to the foam core composites process and therefore does not allow for quick iterative improvement.

## 5.2 Wing

As proposed in the optimization process, the wing is manufactured as a sandwich shell construction. It was decided to manufacture the mold from milled MDF due to the large size of

the wing and the required surface accuracy. A picture of the molds is included in figure 5.1. The layup consist of a fiberglass-layer with a weight of  $40 \frac{\text{g}}{\text{m}^2}$ , a layer of 1.2 mm Airex sandwich material and an inner layer of fiberglass with a weight of  $25 \frac{\text{g}}{\text{m}^2}$ . For simplicity and for conservative estimation, the bending moments are assumed to be carried only by the spar and not by the shell.

Two load cases are considered for the spar design. For the loads during flight, a load factor of  $n = \pm 3$  at a take-off mass of 5.52 kg is considered. In this case the lifting forces are evenly spread over the wing. Also the wingtip test is considered, during which the complete weight of the wing is held on the wing tips, which results in a constant shear stress on the spar. At each point of the wing, the load case causing the greater stress is used to determine the number of rovings. The used rovings IMS65 from Teijin have a tensile strength of 6 000 MPa [7]. Due to uneven alignments during production and a fiber volume ratio of 30% achieved by hand lamination, a tensile strength of 500 MPa is assumed for the roving bundle. The resulting distribution of rovings is shown in table 5.1. The spar shear web consists of vertically aligned balsa wood which is reinforced on both sides with fiberglass fabric of a weight of  $80 \frac{\text{g}}{\text{m}^2}$ .

number of rovings	1	1	1	1	1	1	1	1	3
length [mm]	200	244	280	321	367	420	475	544	1060

**Table 5.1:** IMS65 roving length distribution

The spar joiner is made of two 10 mm × 10 mm CFRP tubes which are inserted into spar pockets in the wings. The pockets are manufactured by wrapping an aramid roving around a positive mold of the spar joiner. The fuselage is connected to the wing by the spar joiner and two additional pins per wing located at the leading and trailing edge of the wing to transfer the torsional loads.



**Figure 5.1:** Molds of the fuselage on the left side and the wings on the right

The wingtip consists of a rib milled from 4 mm thick plywood. The control surfaces are cut from the molded wings and are hinged by aramid fabric which is placed in the outer skin during the shell layup. The aileron and the flaps are controlled by one servo motor each, which is placed inside the wing.

### 5.3 Empennage

For the construction of the empennage, the foam core composites technique was chosen, due to the ease of manufacturing and shorter required production time compared to a shell construction. The drawbacks of foam core composite wings, for example a worse strength-to-weight ratio, are negligible due to the small dimensions of the tail. The control surfaces of the empennage are constructed using aramid hinges which are added to the foam core during the lamination of the carbon fiber skin.

For easy transportation, the empennage is composed of multiple pieces which can be disassembled. The horizontal stabilizer is mounted below a CFRP tube with the outer diameter of 22 mm while the vertical tail plane is mounted on top of the tube. The parts are connected by two M4 bolts going from the bottom of the assembly up into threads in the vertical tail plane. They are placed in 3D printed parts with fitting holes, which are added during the lamination process.

### 5.4 Landing Gear

A tricycle configuration was chosen for the landing gear as mentioned in section 4. Compared to a taildragger configuration, this results in a lower air resistance during take-off acceleration. However, the tricycle configuration leads to a slightly higher mass and drag in flight. Nevertheless, these effects are less significant than the advantages of a shorter take-off distance. The size of the landing gear was designed to allow rotation at take-off with an angle of attack of  $12^\circ$ .

The front landing gear consists of a CFRP-rod which is connected to the fuselage by an aluminum coupler. The wheel is attached to the rod by a spring to dampen unevenness of the airstrip. The rear landing gear is a purchased commercial off-the-shelf CFRP landing gear. It is screwed into the rear baseplate of the fuselage which is connected to the third rib and the wing mounting.

## 5.5 Fuselage

The fuselage contains the payload and the electronic components except the servos. The electronic components are located in the front part of the fuselage to shorten the length of the cables from the electronic speed controller (ESC) to the motor as shown in figure 5.2. Above these components, the measurement box is placed. To ensure a good radio connection, the antenna of the measurement box is not covered by the shell of the fuselage.

Since a tractor configuration was selected as the propulsion configuration, the motor is attached to the front of the fuselage, which is reinforced with a milled plywood frame.

As shown in figure 5.2, the majority of space within the fuselage is taken up by the bloodbags.

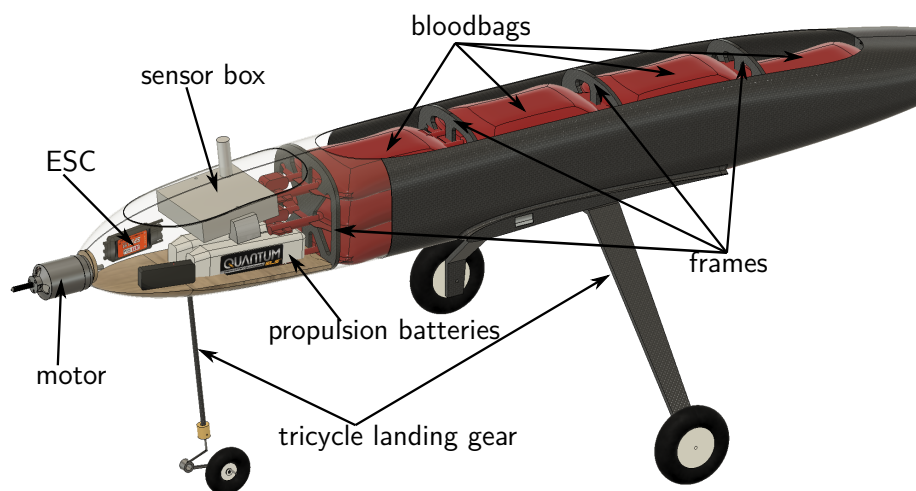


**Figure 5.2:** Placement of the components in the fuselage

Besides securing the payload, the frames additionally reinforce the fuselage. This is particularly necessary because of the large opening cut into the top side for easy loading and unloading.

The CFRP tube, which connects fuselage and tail unit, is removable for easy transportation. The tail tube is inserted into another tube with an inner diameter equal to the outer diameter of the tail tube. The outer tube is firmly glued to the frames of the fuselage. The inner tube is secured to the outer tube by adhesive tape.

Because the required precision is lower and due to the ease of production, 3D printed molds made from polylactic acid (PLA) are chosen for the manufacturing of the fuselage. After the molds are printed, the unevenness between the printing layers must be filled and the molds are polished to the required finish. The frames of the fuselage are milled from sheets of balsa wood reinforced on both side by carbon fiber. Along with all other components, except the electronics and the payload, the frames are glued into the shell of the fuselage.

## 5.6 Payload Prediction

The amount of bloodbags and thus the payload mass was determined by the result of the second optimisation step to 3.346 kg. As stated in the rulebook, the payload should mainly consist of 300 g blood bags. This means that the payload will be split into eleven bags of 300 g ending up very close to the target weight of 3.3 kg. With additional 100 g bags and some additional spare room in the cargo bays the weight can be adjusted if testing shows that a different payload produces a higher point score. The distribution of the blood bags into separate cargo bays was the next step. A few concepts were created with different distributions of the eleven blood bags across different numbers of cargo bays. Combined with the restrictions given by the regulations and the manufacturability of the fuselage, it was determined that four cargo bays are optimal. The payload is packed in stacks of 3-3-3-2 bags across the cargo bays which can be seen in figure 5.2. "CoG pos." in table 5.2 describes the calculated position for the center of gravity of the plane with the corresponding payload. This position is measured from the forward tip of the rhombus shape provided by the regulations.

	Bay 1	Bay 2	Bay 3	Bay 4	CoG pos.
Max. payload configuration	900 g	900 g	900 g	600 g	938 mm
Min. payload configuration	-	-	-	500 g	928 mm

**Table 5.2:** Payload Configurations

As stated in the rules, the linear function for calculation of the payload  $m_{\text{payload}}$  [kg] over air density  $\rho$  [ $\frac{\text{kg}}{\text{m}^3}$ ] is given with formula 5.1. The corresponding graph is given in figure 5.3.

$$m_{\text{payload}}(\rho) = 0.66 + 2.19 \cdot \rho \quad (5.1)$$

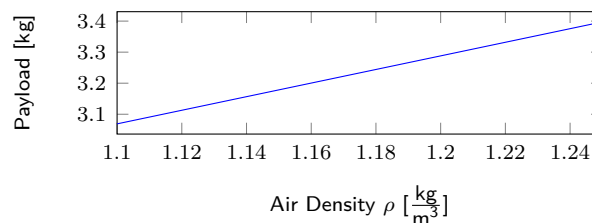


**Figure 5.3:** Payload prediction as a function of the air density  $\rho$

## 6 Electronic Components

This chapter describes the selection of electronic components that are not specified by the regulations.

### 6.1 Battery

The goal of selecting a particular battery is to achieve maximum electric power in flight. First, a selection of four possible LiPo batteries from different manufacturers was made. Table 6.1 shows the LiPo batteries available for selection together with their manufacturer specifications.

	Name	Nominal voltage	Capacity	C-rate
(1)	SLS Quantum	11.1 V	2.2 A h	65 h <sup>-1</sup>
(2)	Dinogy Graphene 2.0	11.1 V	2.2 A h	70 h <sup>-1</sup>
(3)	Turnigy Graphene Panther	11.1 V	2.2 A h	75 h <sup>-1</sup>
(4)	Turnigy Bolt HV	11.4 V	2.2 A h	65 h <sup>-1</sup>

**Table 6.1:** Manufacturer's specifications of the tested batteries

Battery (4) has a higher nominal voltage and can therefore be charged to a higher voltage. Since the maximum starting voltage is specified in the regulations as 12.6 V, battery (4) must not be charged to the maximum voltage. In the following, discharge tests were performed with a static ground test. Figure 6.1 shows the different discharge curves of the batteries with the ESC at 100% throttle in a time interval of 180 s. The time interval of 180 s was chosen to represent the 60 s climb and the 120 s cruise flight. Figure 6.1 shows that battery (3) has a minimally higher voltage level than battery (1) and is therefore used.

### 6.2 Servomotors

The servo motors should be as light as possible and must fit into the wing structure. The selection of the servos is based on the calculation of the maximum forces on the flaps and

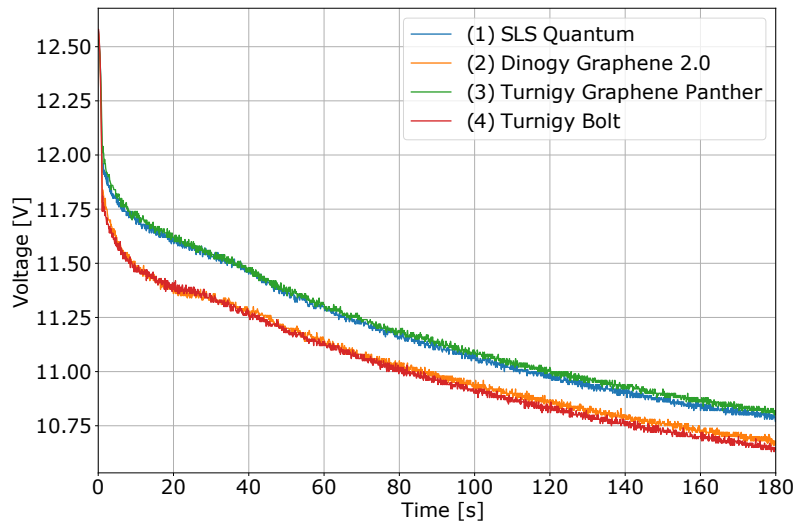


**Figure 6.1:** The voltage  $U$  of the four batteries examined at full thrust plotted over time

control surfaces. The calculation of the required torque takes the control surface dimensions, the maximum deflection, the wing chord length and the airspeed into account as shown in table 6.2. As a safety margin we searched servos with at least 1.5 times the required values. Although we would only need servos with about 2.6 kg cm for the ailerons and tail surfaces, the KST X08H Plus is the smallest available servo in its class and is therefore used despite its excessive capabilities. For the flaps, the KST X10-710 was the best option, because its rated 7.5 kg cm perfectly matched our needed 7.41 kg cm.

	Flaps	Ailerons	Rudder/Elevators
Speed	110 $\frac{\text{km}}{\text{h}}$	110 $\frac{\text{km}}{\text{h}}$	110 $\frac{\text{km}}{\text{h}}$
Flaps max deflection	45°	45°	45°
Flaps depth	67 mm	50 mm	50 mm
Flaps width	550 mm	340 mm	200 mm
Avg. chord length flaps	285 mm	230 mm	200 mm
Needed torque	4.94 kg cm	1.75 kg cm	0.98 kg cm

**Table 6.2:** Parameters and results of the torque calculation

## 7 Testing

Wind tunnel tests were conducted to validate the calculation of the powertrain. In figure 7.1, the assembly of the custom thrust test stand in the wind tunnel is shown.

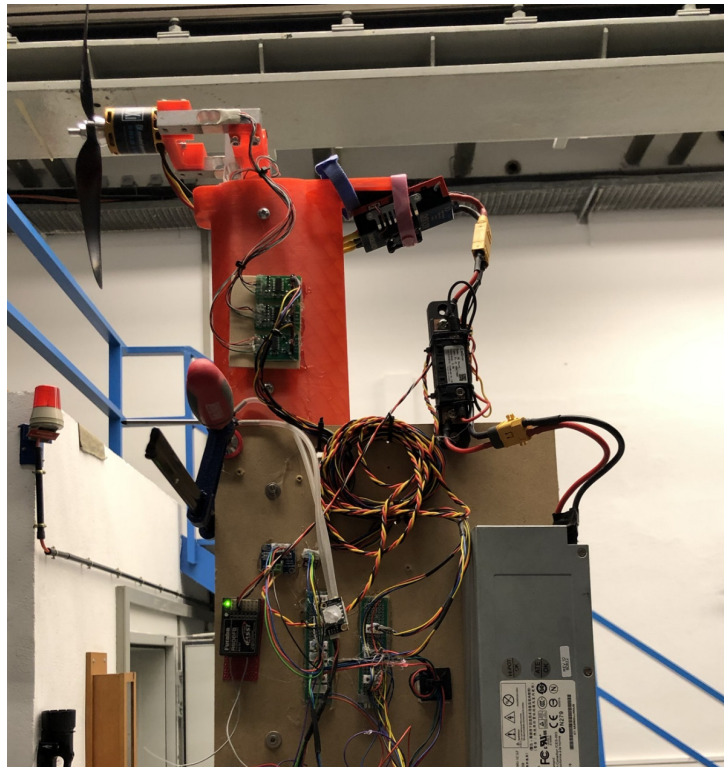


**Figure 7.1:** Thrust test stand in the wind tunnel

The tests helped us with the following aspects:

1. Propeller selection (APC vs. CAM)
2. Battery selection (described in section 6.1)
3. Validation of QPROP calculations
4. Determination of battery voltage levels for take-off, climb and cruise

## 7.1 Propeller Selection

In accordance with the regulations, the CAM-Carbon Light-Prop 10x6 or APC 10x6 E propellers can be used. Figure 7.2 shows the results of the wind tunnel tests in a speed range from 0 to 16 m/s. The motor was operated with a 12V power supply unit. It can be clearly seen that the CAM propeller generates more thrust and is therefore selected as the only propeller in the plane development process.

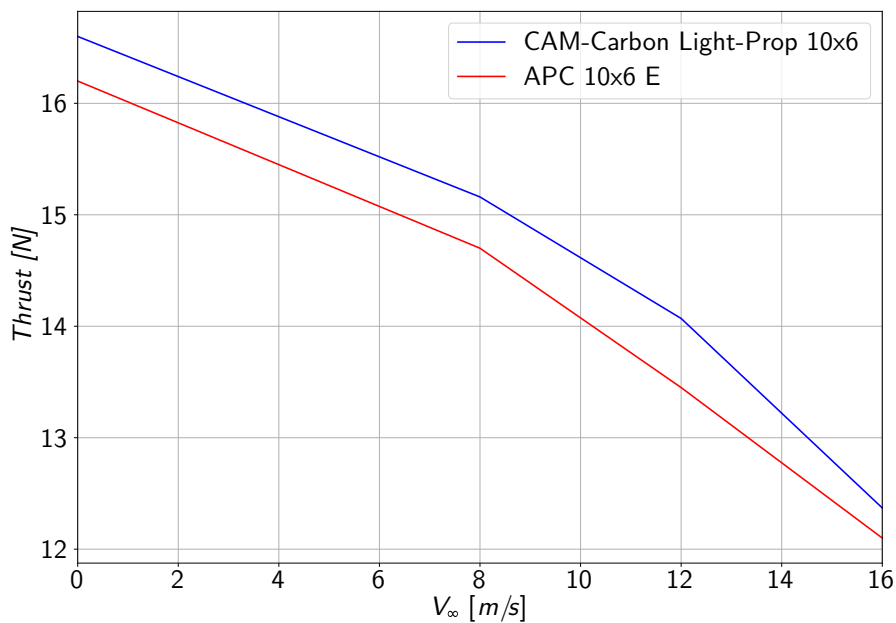


**Figure 7.2:** Comparison of the propeller thrust over a speed range from 0 to 16 m/s.

## 7.2 Validation of QPROP calculations

To validate of the QPROP results, a power supply with an output voltage of 12V was used. In figure 7.3 the thrust is plotted over the inflow velocity  $V_\infty$ . It is shown that the thrust calculated with QPROP is clearly above the thrust measured. For this reason a correctional function 7.1 was created.

$$F_{\text{corr}} = a \cdot F_{\text{QPROP}} - \frac{V_\infty - b}{c} \quad (7.1)$$

With  $a = 0.84$ ,  $b = 11 \frac{\text{m}}{\text{s}}$  and  $c = 11 \frac{\text{s}}{\text{kg}}$ , the corrected thrust curve is shown in figure 7.3. The comparison at different operating voltages results in a maximum thrust deviation of 0.5 N

between QPROP calculations and test results. Thus, the correction equation 7.1 with the parameters  $a$ ,  $b$  and  $c$  is a sufficiently accurate estimate for the thrust calculation.

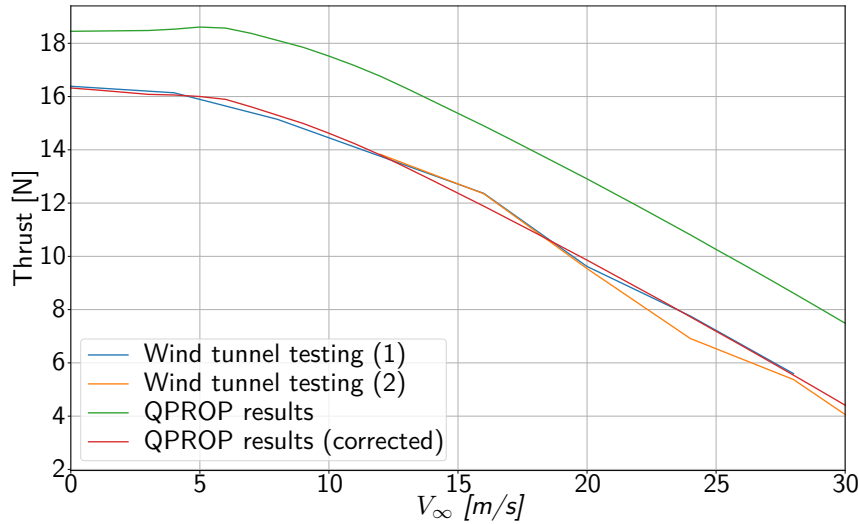


**Figure 7.3:** The thrust  $F$  from wind tunnel testing, the QPROP calculation, and the corrected QPROP calculation plotted versus  $V_\infty$ .

### 7.3 Determination of voltage levels depending on battery capacity

Further tests were carried out to determine the voltage levels of take-off, climb and cruise. A constant voltage level is determined for each of these three flight phases. The respective voltage level depends mainly on the battery capacity. Figure 7.4 shows the results of the discharge tests. The data points for take-off are obtained in each case by averaging the voltage in the first 10 s. The data points for the climb result analogously for the time interval  $10\text{ s} < t < 60\text{ s}$ . For cruise, the voltages are averaged over the time interval  $60\text{ s} < t < 120\text{ s}$ . The data points are approximated with the logarithmic function

$$y = a \log(x) + b. \quad (7.2)$$

For take-off, climb and cruise, the parameters  $a$  and  $b$  with the standard deviations  $\sigma$  from the measured values are given in table 7.1.

	$a$	$b$	$\sigma$
Take-off	-0.262388	12.665194	0.06733 V
Climb	-0.399414	12.716106	0.05540 V
Cruise	-0.613793	12.743069	0.03603 V

**Table 7.1:** Parameters determined through testing for logarithmic function 7.2

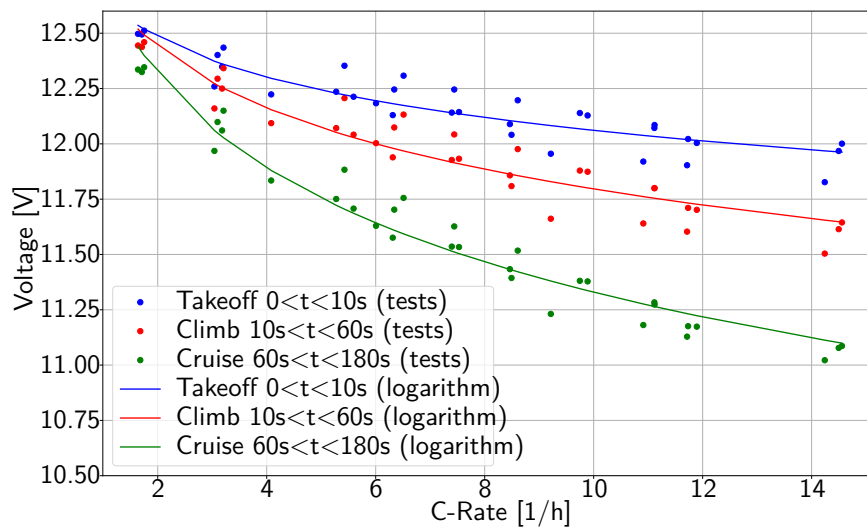


**Figure 7.4:** The measured data points of the averaged voltage at take-off ( $t < 10s$ ), climb ( $10s < t < 60s$ ) and cruise ( $60s < t < 180s$ ) and the respective function approximated by the logarithm.

## 8 Outlook

This chapter covers the steps required to be fully prepared for the competition. The Air Cargo Challenge will be in July, resulting in about two-and-a-half months left for these steps. There are several difficulties to deal with over the next months. These obstacles affect various assemblies of the aircraft which are described as follows.

We are in the middle of manufacturing the prototype, with the wing still requiring the most work. The wing shells are already laminated, but still have to be joined. The connection to the fuselage needs to be integrated and the control surfaces have to be cut free and actuated. In contrast to the wing, the construction of our fuselage is already progressed much further. The empennage has been manufactured; only the servo motors still need to be integrated and assembled finally.

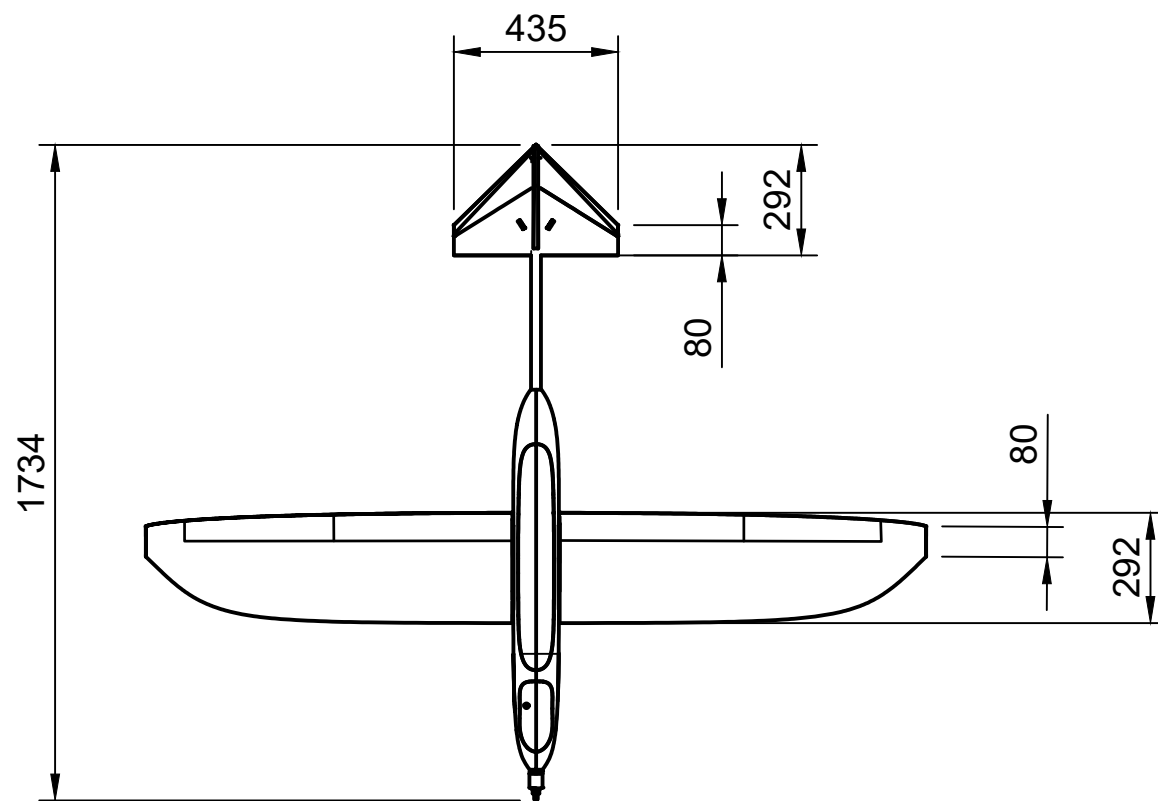
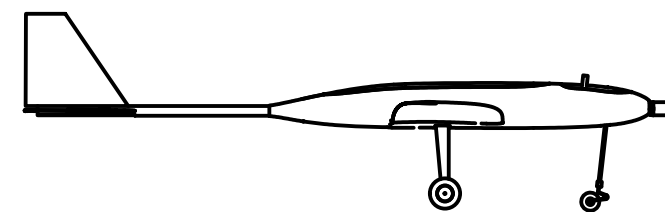
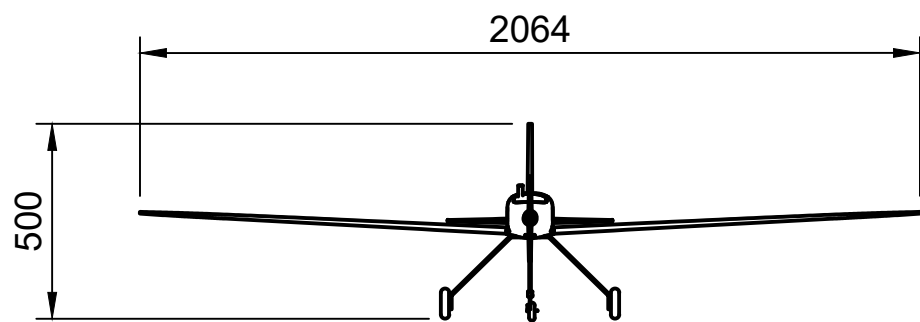
As soon as the manufacturing of the prototype is completed, test flights will be conducted. We are going to test all aircraft systems as well as the aircraft performance and try to identify areas for further improvements. Furthermore, our pilots have to familiarize themselves with the aircraft's handling characteristics in order to fly the optimal flight path.

If we still have time, we want to replace the off-the-shelf landing gear with one we will develop ourselves. This has potential to save mass and improve aerodynamics. To reduce the rolling resistance, we want to test different wheels, for which a test rig has already been developed. Finally, the results of these tests are to be incorporated into the final competition aircraft, which is also to be manufactured in an even lighter design.

As described in this chapter, besides the already manufactured components, some tasks still need to be completed to be ready for the Air Cargo Challenge in July. We will have to put in some more work, but are optimistic that the remaining time is sufficient and we are all looking forward to the competition in Munich.

# Bibliography

- [1] ANDERSON, J. D.: Introduction to flight. McGraw-Hill series in aeronautical and aerospace engineering, New York, NY: McGraw-Hill Education, ISBN 978-0-07-802767-3, 2016.
- [2] DRELA, M.: QPROP, <http://web.mit.edu/drela/Public/web/qprop/> (accessed December 12, 2021), 2007.
- [3] DRELA, M.; YOUNGREN, H.: AVL, <http://web.mit.edu/drela/Public/web/avl/> (accessed December 14, 2021), 2004.
- [4] DRELA, M.; YOUNGREN, H.: XFOIL, <https://web.mit.edu/drela/Public/web/xfoil/> (accessed December 12, 2021), 2001.
- [5] LENNON, A.: Basics of R/C model aircraft design. Practical techniques for building better models, Wilton, Connecticut: Air Age, ISBN 0-911295-40-2, 2005.
- [6] RAYMER, D. P.: Aircraft Design. A Conceptual Approach, Washington, D.C.: AIAA Education Series, ISBN 0-930403-51-7, 1989.
- [7] TEIJIN CARBON EUROPE GMBH: Tenax™ Filamentgarn, <https://www.tejincarbon.com/de/produkte/tenaxr-kohlenstofffaser/tenaxr-filamentgarn?r=1> (accessed April 14, 2022).
- [8] THIES, W.: Handbuch für den Modellflug. Band 1: Entwurf und Planung von RC-Segelflugmodellen, Baden-Baden: Verlag für Technik und Handwerk GmbH, ISBN 3-88180-000-X, 1982.
- [9] TORENBECK, E.: Advanced aircraft design. Conceptual design, analysis, and optimization of subsonic civil airplanes. Aerospace series, Chichester: Wiley, ISBN 978-1-118-56811-8, 2013.



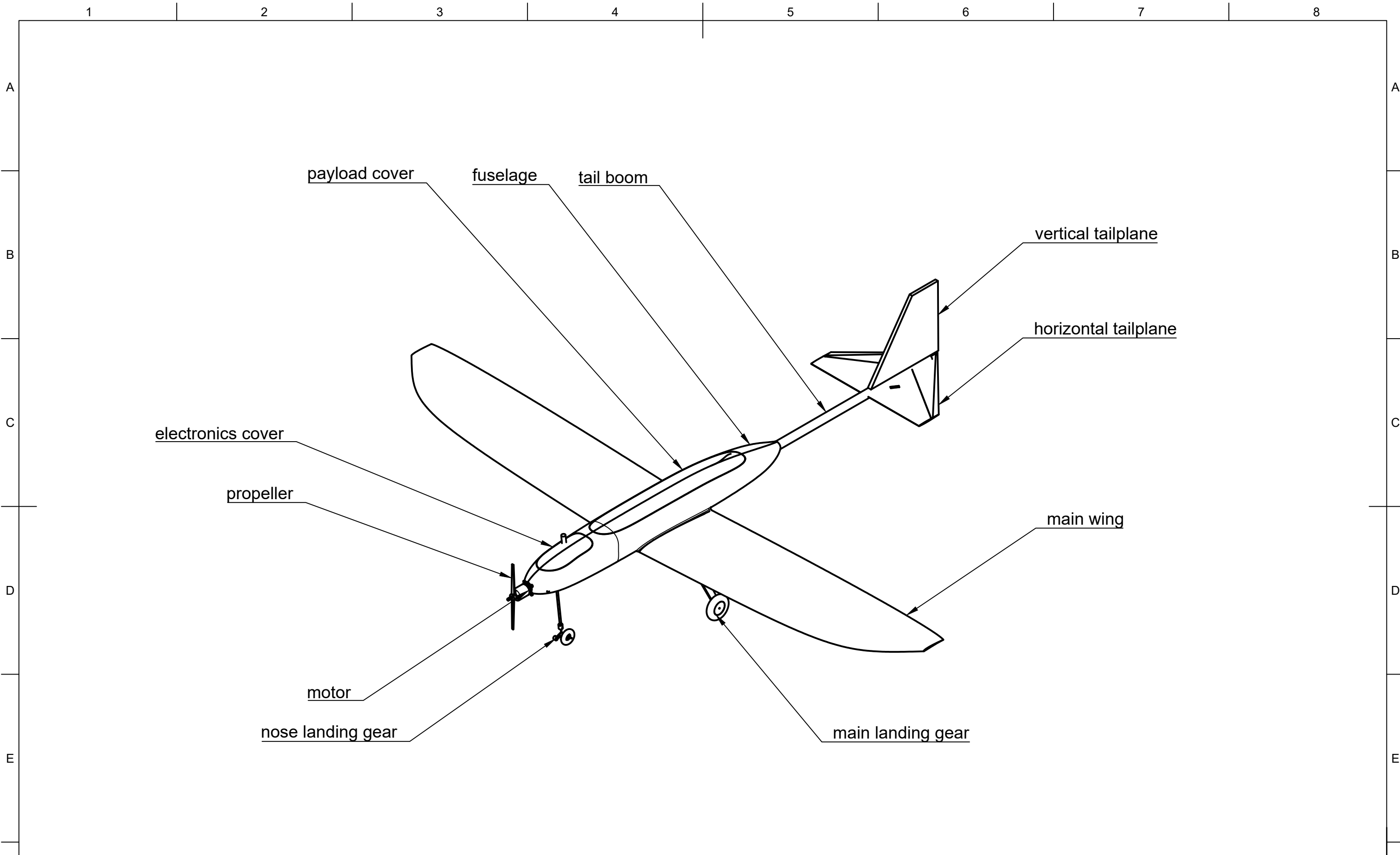
Airplane Data	
wing area [m <sup>2</sup> ]	0,534
wing airfoil	ag19
wing loading [g/dm <sup>2</sup> ]	103.39
epennage airfoil	goe443
flap dimensions [mm <sup>2</sup> ]	550x67
aileron dimensions [mm <sup>2</sup> ]	340x50
rudder/elevator dimensions [mm <sup>2</sup> ]	200x50
vertical velocity during climb [m/s]	1.82
cruise velocity [m/s]	27.4
body volume [dm <sup>3</sup> ]	10.12
plane mass [kg]	5.626



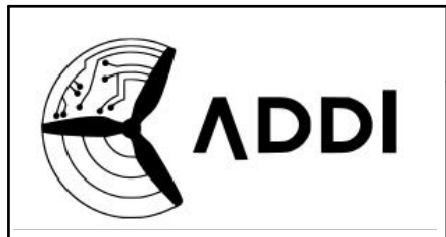
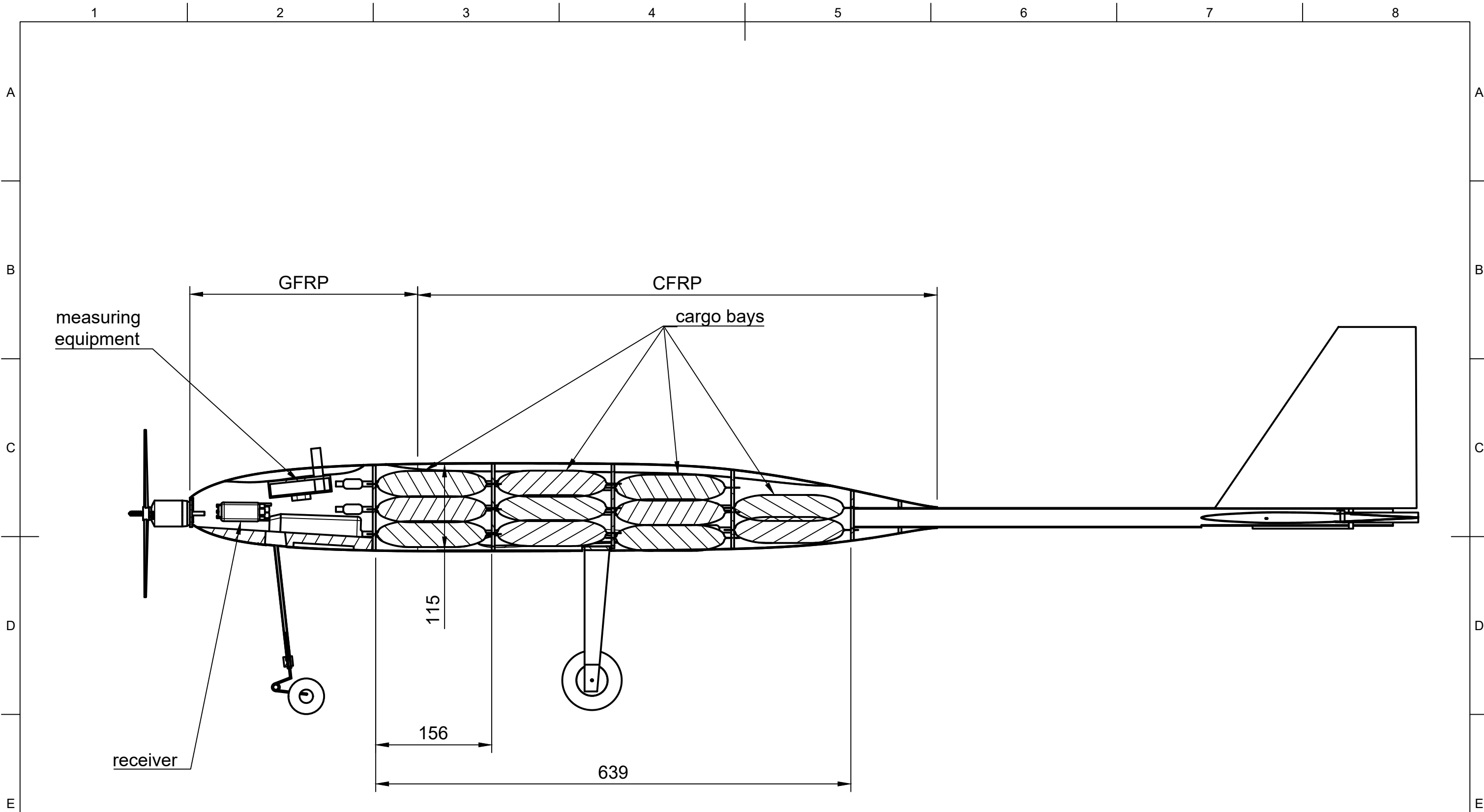
Team number	13	Scale	1:20
-------------	----	-------	------

Title	Airplane Assembly	Drawing type	3-view drawing
-------	-------------------	--------------	----------------

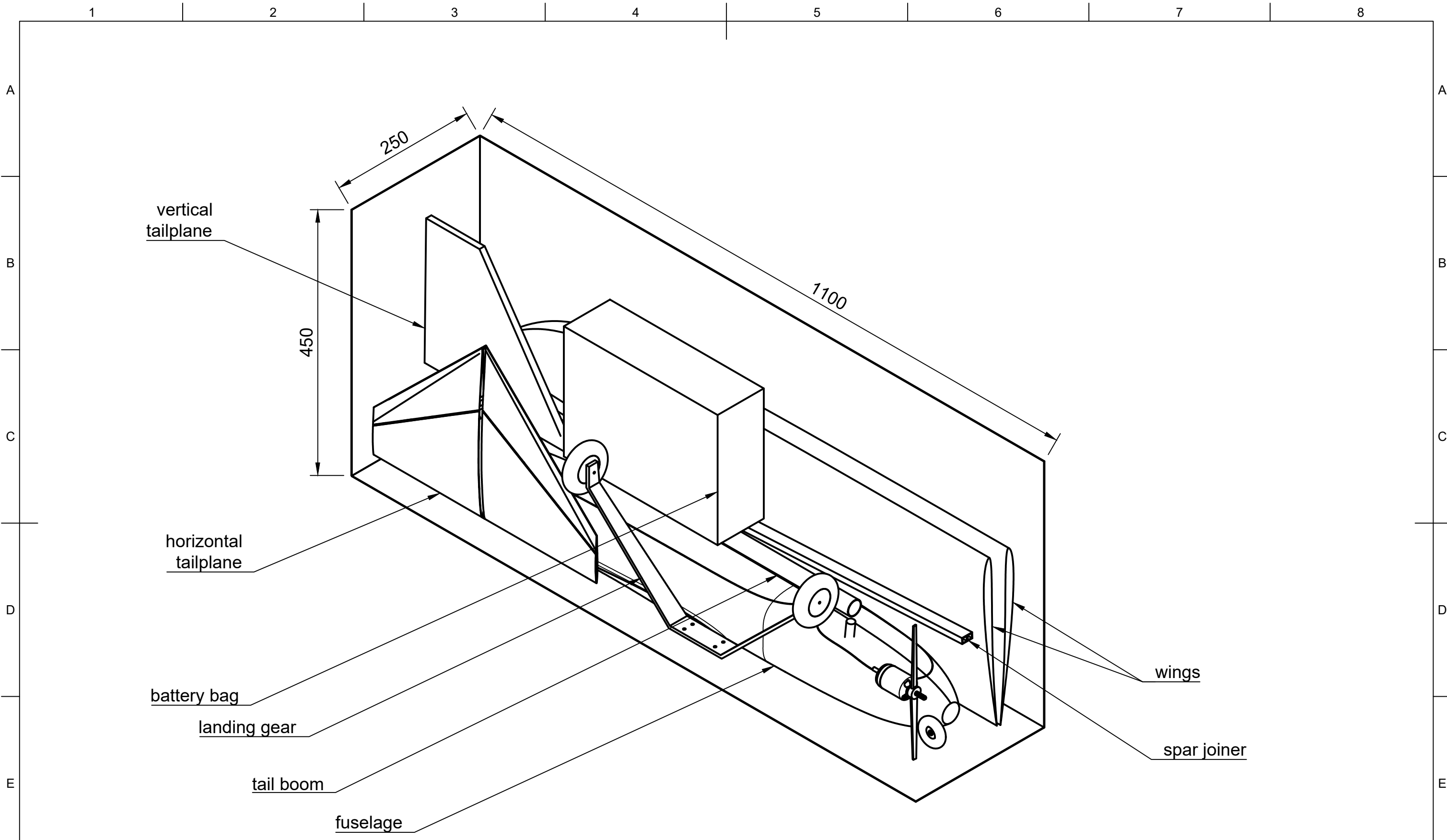
Rev.	Date of issue	Sheet
------	---------------	-------



	Team number	13	Scale	1:10
	Title		Drawing type	
	Airplane Assembly		isometric drawing	
Rev.	Date of issue	Sheet		



Team number <b>13</b>	Scale <b>1:5</b>
Title <b>Airplane Assembly</b>	Drawing type <b>Cargo bay, receiver position, measuring equipment position</b>
Rev.	Date of issue
	Sheet



	Team number	Scale
	13	1:5
	Title	
Airplane Assembly		Drawing type
		transportbox-packaging
Rev.	Date of issue	Sheet